Analysis of Volcanic Lightning and Eruption Column Development During the April 2021 Eruption of La Soufrière, St. Vincent

Tuba Minhas

Department of Atmospheric, Oceanic and Planetary Physics

University of Oxford

Summer internship report

July 2025

Supervisor - Dr. Isabelle Taylor

Abstract

This study examines volcanic lightning and cloud dynamics during the April 2021 explosive phase of the La Soufrière, St. Vincent, eruption, with a focus on the highly active Event 17. Lightning detection data from the World Wide Lightning Location Network (WWLLN) were integrated with high-temporal-resolution satellite observations from the GOES-16 Advanced Baseline Imager (ABI) to investigate eruption onset, eruption column evolution, and electrification processes. Analysis involved spatial and temporal correlation of lightning strikes with the eruption column development, as well as parallax corrections to assess plume height from lightning positions. Atmospheric forecasts provided by the European Centre for Medium Ranged Weather Forecasting (ECMWF) were used to assess meteorological influences on lightning activity. Event 17 exhibited anomalously high lightning rates compared with other events, likely linked to source intensity rather than atmospheric variability. Possible mechanisms include enhanced ash fragmentation, increased charging efficiency, and pyroclastic density current–related electrification. While WWLLN's detection efficiency limitations constrained the completeness of the dataset, results demonstrate the potential of combining volcanic lightning monitoring with satellite data to characterise eruption dynamics, identify ash-bearing plumes, and improve operational eruption detection capabilities.

1 Introduction

Soufrière St. Vincent (also referred to as "La Soufrière") is the northernmost stratovolcano on St. Vincent Island in the southern part of the Lesser Antilles volcanic arc, reaching a height of 1220 m with a summit crater 1.6 km in diameter and 300–600 m deep [1] [2]. St. Vincent is the largest island within Saint Vincent and the Grenadines (SVG), an island nation in the eastern Caribbean situated in the Windward Islands of the Lesser Antilles. The country lies at the southern end of the eastern boundary between the Caribbean Sea and the Atlantic Ocean, with Saint Lucia to the north, Barbados to the east, and Grenada to the south. The geographical setting of both the country and the volcano is shown in Figure 1. Recorded eruptions date back to 1718, with notable eruptions occurring in 1812, 1902, and 1979 [1]. La Soufrière entered a major phase of explosive eruptions on 9 to 22nd April 2021, following an initial phase of an effusive activity that began on 27 December 2020, with the growth of a new lava dome on the SW edge of the main crater [2] [1].

Taylor et al., 2023 identified a minimum of 35 eruptive events using true- and false-colour images and brightness-temperature difference maps by using satellite instruments such as the Advanced Baseline Imager (ABI) [3]. Understanding the 2021 La Soufrière eruption and its associated geophysical phenomena is crucial for improving volcanic hazard assessments and enhancing preparedness and response strategies in volcanically active regions. This study investigates volcanic lightning as a means to determine the start and end times of eruptive events, as well as to estimate plume height and ascent rates. Ground-based instruments, including the World Wide Lightning Location Network (WWLLN), were used to collect lightning data in the region through the Global Volcanic Lightning Monitor programme, which collects data on a majority of volcanoes across the globe.

1.1 Lightning

Lightning is a transient, high-current electrostatic discharge that occurs when the electric field between two regions exceeds the dielectric strength of air, typically around 3 $\mathrm{MV\,m^{-1}}$ [4]. In thunderclouds, charge separation is primarily driven by collisions between supercooled water droplets, ice crystals, and graupel, producing a characteristic charge structure [4]. Three principal discharge types are observed: intra-cloud (IC), which occurs between charge regions within the same cloud; cloud-to-cloud (CC), which connects separate clouds; and cloud-to-ground (CG), which transfers charge between a cloud and the Earth's surface. CG flashes may be negative, by far the most common, or positive, which are rarer but can produce peak currents exceeding 100 kA [4].

To illustrate these processes in more detail, cloud-to-ground lightning provides a clear example. Its development typically begins with the formation of a stepped leader, a branching, downward-propagating channel of ionised air that advances in discrete steps of tens of metres. When this

Figure 1: Geographical location of Saint Vincent and the Grenadines within the Lesser Antilles (left), with an inset showing the island of Saint Vincent and the location of La Soufrière volcano (black triangle). Basemap imagery is from Google Maps; figure compiled by the author.

leader approaches the ground, upward streamers are launched from elevated objects, and once contact is made, a high-current return stroke propagates upward along the channel, producing the bright visible flash [4]. This sequence of leader–streamer interaction followed by a return stroke is often repeated several times along the same channel, resulting in multiple strokes within a single lightning flash. Figure 2 illustrates the stepped leader and return stroke process schematically.

2 Instruments

2.1 WWLLN: Global Volcanic Lightning Monitor

The World Wide Lightning Location Network (WWLLN) is a global array of around than 70 very low-frequency (VLF) sensor stations that timestamp the Time of Group Arrival (TOGA) of lightning 'sferics', which are a burst of radio waves emitted by lightning, and apply multilateration, requiring at least five station detections, to geolocate strokes [6]. Multilateration is the process of determining the location of points by measuring distances from known points [7]. The adoption of the TOGA algorithm and expansion to more stations have reduced the global median

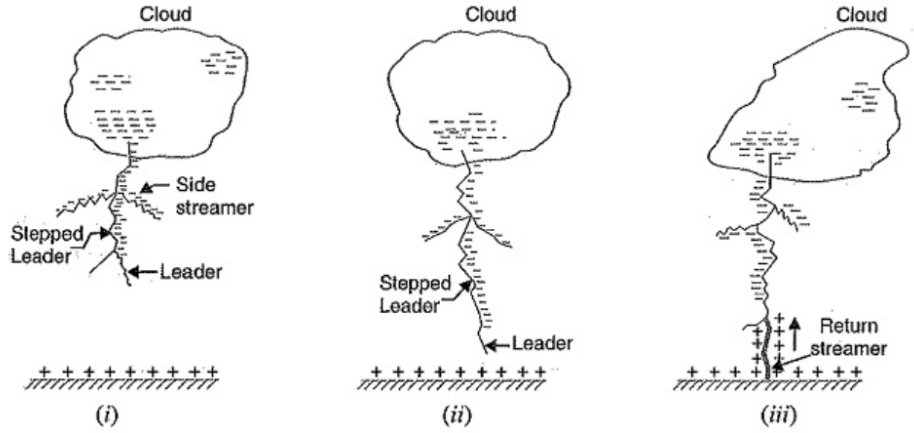

Figure 2: Schematic representation of cloud-to-ground lightning development showing the stepped leader, upward streamers, and return stroke [5].

location error to approximately 2.9 km (mean 3.4 km) [8]. In addition to mapping thunderstorm activity in near real time, WWLLN operates an experimental Ash Cloud Monitor (ACM) volcanic lightning programme, which issues alerts when clusters of VLF pulses are detected within defined radii (20 km and 100 km) around active volcanoes [9]. The resulting Global Volcanic Lightning Monitor provides minute-by-minute flash counts for each volcano within both an inner and outer radius, offering volcanologists timely, remote insight into plume electrification and eruption dynamics [10]. The data used in this study is freely available through this link here: `https://wwlln.net/USGS/Global/`.

2.2 Advanced Baseline Imager

The Advanced Baseline Imager (ABI) is the primary instrument aboard the GOES-R Series for imaging Earth's weather, oceans, and environment. ABI views the Earth with 16 different spectral bands, including two visible channels, four near-infrared channels, and 10 infrared channels spanning the 0.45 to 13.7 μm spectral range [11] [12]. This range is useful for tracking volcanic plumes as the 8.5 and 7.34 μm bands are the primary bands for detecting sulfur dioxide (SO_2), which is an abundant gas in volcanic eruptions [13] [12]. The ABI on GOES-16 typically records full-disc images every 10 minutes [11]. However, it is also equipped with two moveable mesoscale sectors, each covering an area of 1000 $\times$ 1000 km at the sub-satellite point, and which can provide images every 60 seconds [14]. During the eruption of La Soufrière, one of these mesoscale regions was repositioned to cover the volcano, allowing for high temporal resolution observations of the event [3].

3 Methodology and Results

3.1 Integration of WWLLN Lightning and ABI Observations

The WWLLN provides KML files containing information on the coordinates of lightning strikes, the corresponding UTC times, and the residual timing, which is the error associated with the detection and the delay between the strike and its registration by the network (found here `https://wwlln.net/USGS/Global/`). The strikes are categorised based on their distance from the volcano's summit: either within a 20 km radius or between 20 km and 100 km. The residual timing errors are typically on the scale of microseconds or nanoseconds and are therefore considered negligible in this study. Although these KML files can be imported into Google Earth to generate interactive plots, a different approach was taken. The KML data were instead imported into Python, and packages such as CartoPy were used to visualise the lightning strike locations relative to the island. A colourmap was applied to distinguish between strikes occurring earlier in the day and those occurring later in the evening, as can be seen in Figure 3.

Figure 3 illustrates the lightning activity observed during the first four days of the volcanic eruption, spanning 9–12^{th} April 2021. The spatial distribution and temporal evolution of lightning strikes are clearly depicted. On 9^{th} of April, lightning activity was limited, with strikes occurring primarily within 20 km of the volcano's summit. By 10^{th} of April, activity intensified, and the strikes exhibited a plume-like east-northeastward dispersion, likely reflecting the influence of prevailing atmospheric winds on ash transport. Lightning peaked on 11^{th} April, with a high concentration of strikes observed both within the 20 km and 100 km buffer zones, particularly clustered around the summit. This elevated activity may correspond to more intense eruptive phases, suggesting enhanced convective dynamics within the ash plume and the activation of electrification mechanisms. On 12^{th} of April, lightning frequency declined markedly, accompanied by a northward spatial shift in activity. This change may reflect a reduction in eruptive intensity, altered plume dynamics, or evolving meteorological conditions. From this point onwards, the frequency of lightning strikes had significantly decreased. Figure 4 presents similar information to Figure 3, but in quantitative form. It is evident that on 11^{th} April there were approximately 300 strikes within the 20 km buffer zone, after which the number of strikes within this zone decreased significantly.

Taylor et al. [3] identified a minimum of 35 eruptive events using a combination of true colour, false colour, and brightness temperature difference maps derived from the ABI data [3]. In this study, brightness temperature maps corresponding to events 6 through 33 (as referred to in [3]) were used. The detection times of each event in UTC+00:00 is shown in Table 1. Using these start times and the associated number of lightning strikes, Figures 5 and 6 were produced to show the lightning frequency per event between 9^{th} and 14^{th} April. The figures illustrate both the number of strikes associated with each event and the duration of each event as determined by Taylor et al. [3]. The colour scheme indicates the eruptive phases: initial eruption (red), sus-

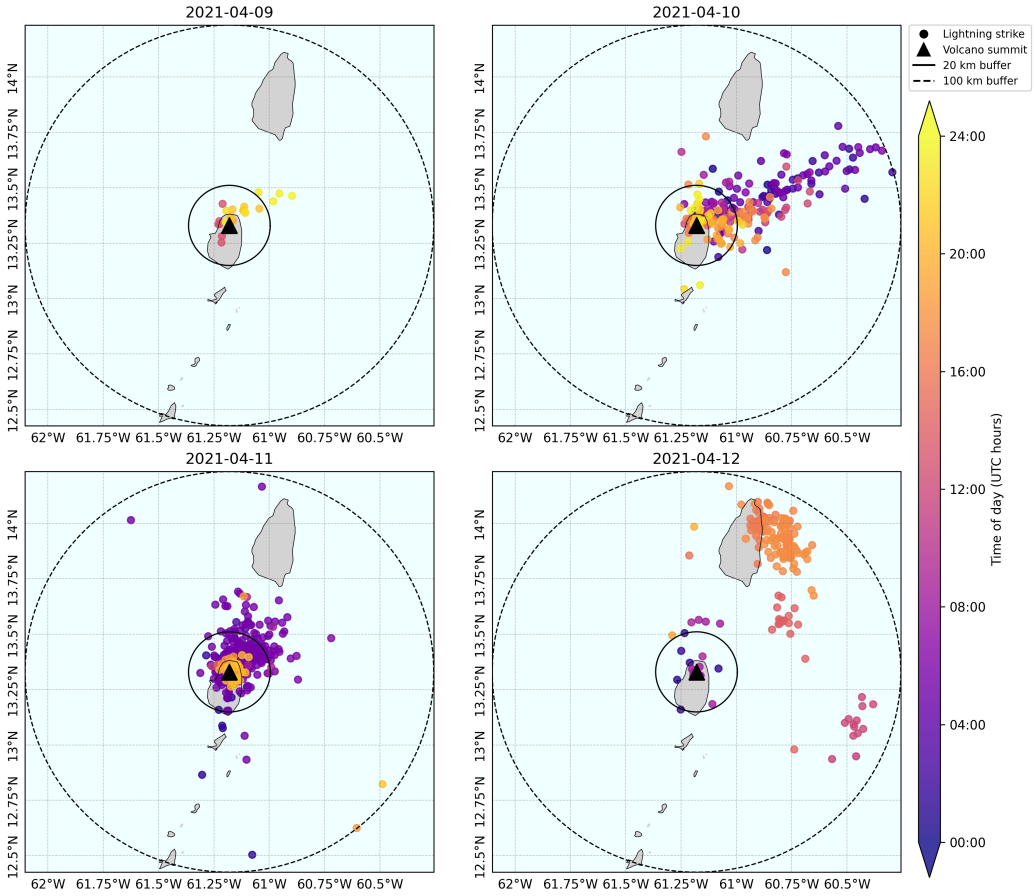

Figure 3: Spatial and temporal distribution of volcanic lightning detected by WWLLN during 9–12 April 2021. Circles indicate 20 km and 100 km buffers around La Soufrière's summit (black triangle). Points are coloured by UTC time of day, showing changes in lightning location and intensity throughout the eruption.

tained eruption (orange), pulsatory phase (purple), and waning phase (pink). From the figures, Phase 2 exhibited sustained lightning activity with variable frequency, a trend that continued into the pulsatory phase on 10^{th} April. One event in particular, Event 17, is notable for its elevated activity compared with the relatively minimal lightning observed on 11^{th} April. The overall decreasing trend persisted until a sharp peak on 12^{th} April, which does not appear to be associated with any eruptive event. During the waning phase, lightning strikes were primarily associated with the onset of eruptive activity.

Combining these plots, it was hypothesised that the shape and distribution of lightning strikes reflects the morphology of the volcanic plumes. This interpretation is supported by the plume-like patterns evident in the lightning data, as well as the tendency for lightning to coincide with the onset of eruptive events. To investigate this, the spatial distribution of lightning strikes was overlaid onto minute-by-minute ABI data (pre-processed by Isabelle Taylor) from which bright-

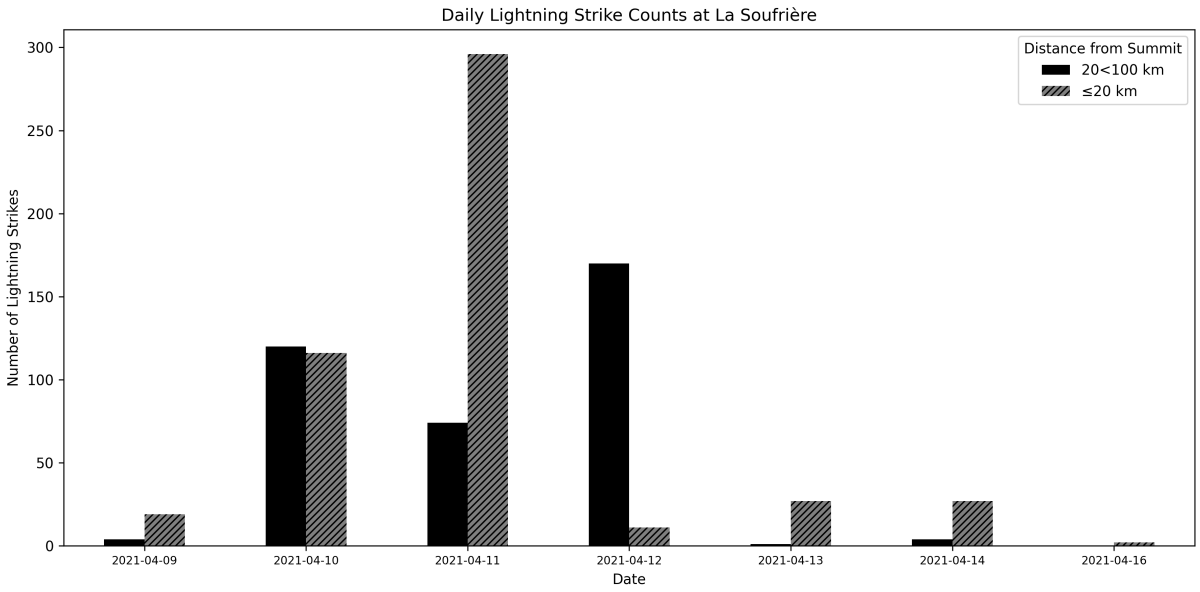

Figure 4: Daily lightning strike counts at La Soufriere between 9^{th} and 16^{th} April. Bars indicate lightning within the 20 km and 20-100 km around the summit.

ness temperature maps were generated. The Python script developed to generate brightness temperature difference maps was obtained, and the start time of each event was entered, with a duration of 90 minutes selected for each sequence. Lightning strike coordinates were then matched to those in the brightness temperature maps to assess whether they aligned with the plume-like patterns observed in the thermal data.

For most events, the frequency of lightning strikes during a given time period was observed to be relatively low, and there appeared to be a delay between the onset of the eruption, as seen in the plume development, and the detection of the first lightning strike, like in Event 11 in Figure 8. Event 17, stood out due to the unusually high number of strikes, 43, occurring within the first $2 - 7$ frames as seen in Figure 7. Strikes are detected before any significant ash is ejected, a pattern that is not seen in the other events. The unusually high density of flashes in the first few minutes is also anomalous to other events. In contrast, Figure 8 (Event 11, same frames) exhibits a drastically fewer lightning strikes, despite the fact that there is a plume development appears similar to Event 17. Based on the ABI data alone, it was not possible to determine why Event 17 differed so much from the others. Addressing this question required a deeper understanding of lightning dynamics and the charging mechanisms responsible for lightning generation, and whether the necessary atmospheric and eruptive conditions were met during the course of the observed volcanic activity.

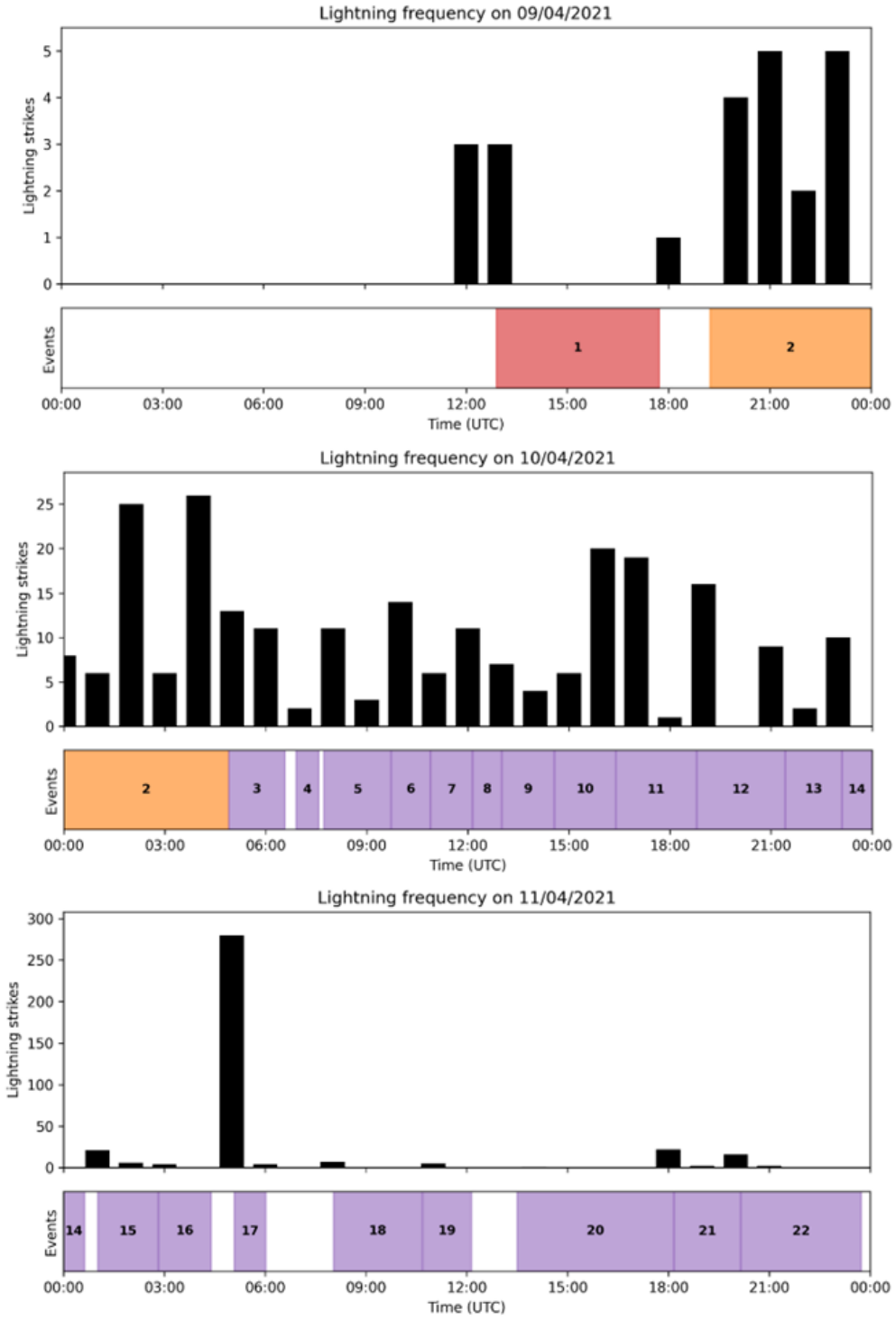

Figure 5: Lightning frequency per event for 9^{th} to 11^{th} April. The coloured boxes show the duration of the events and what phase the eruption was in: initial eruption (red), sustained eruption (orange), pulsatory phase (purple) [3].

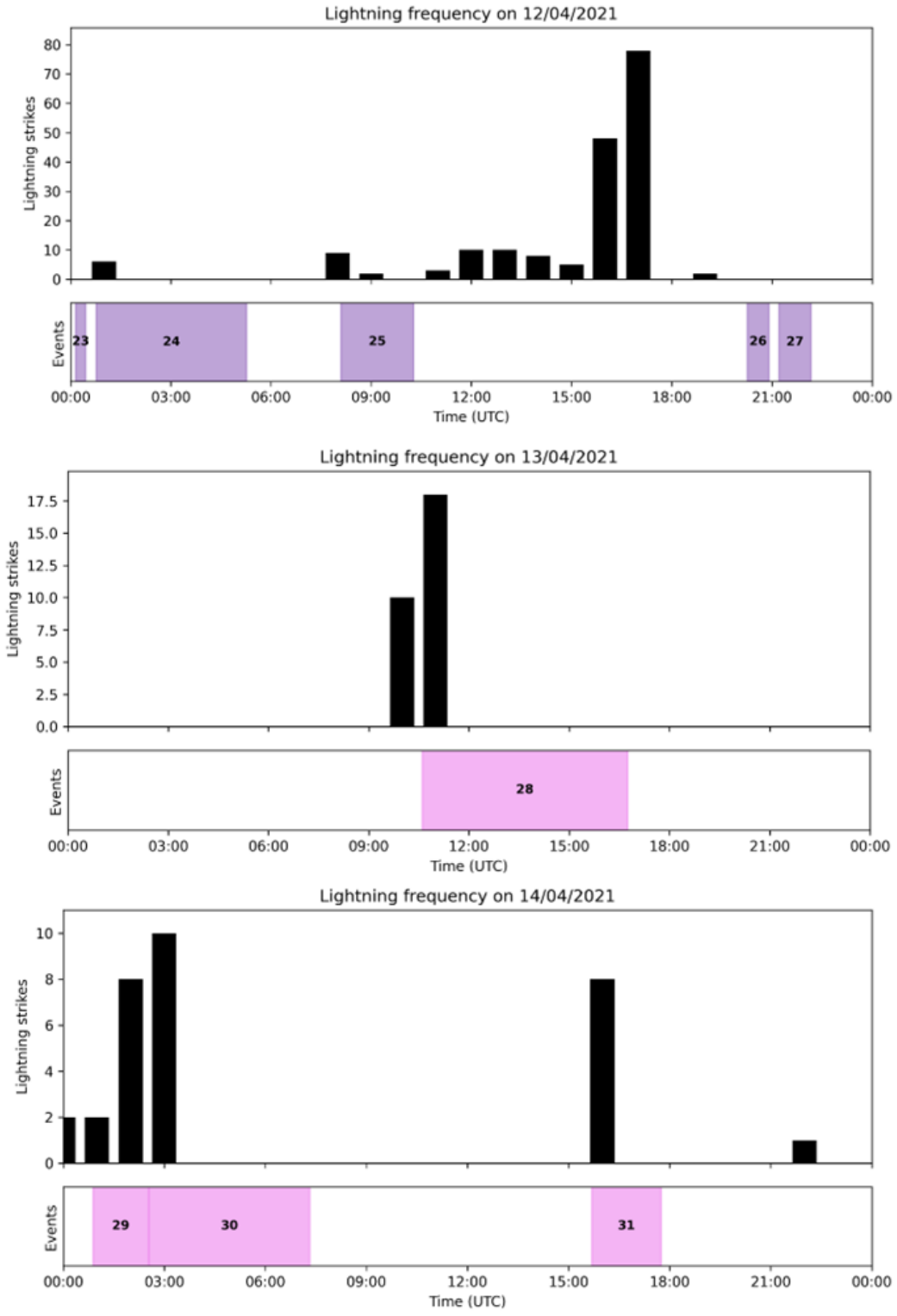

Figure 6: Lightning frequency per event for 12^{th} to 14^{th} April. The coloured boxes show the duration of the events and what phase the eruption was in: pulsatory phase (purple), waning phase (pink) [3].

Table 1: Event detection times and lightning strike counts within 100 km for 33 events identified by Taylor et al. during April 2021 [3]. Times are given in UTC+00:00.

Event	**Day**	**Detection Time (HH:MM)**	**Number of Lightning Strikes**
6	10	09:44	19
7		10:54	15
8		12:09	13
9		13:01	9
10		14:35	8
11		16:24	39
12		18:48	17
13		21:26	11
14		23:07	10
15	11	01:01	21
16		02:50	8
17		05:05	284
18		08:02	7
19		10:42	5
20		13:30	1
21		18:10	21
22		20:09	18
23	12	00:09	6
24		00:46	6
25		08:06	11
26		20:16	0
27		21:13	0
28	13	10:36	28
29	14	00:53	10
30		02:33	11
31		15:41	8
32	15	08:58	0
33	16	10:44	0

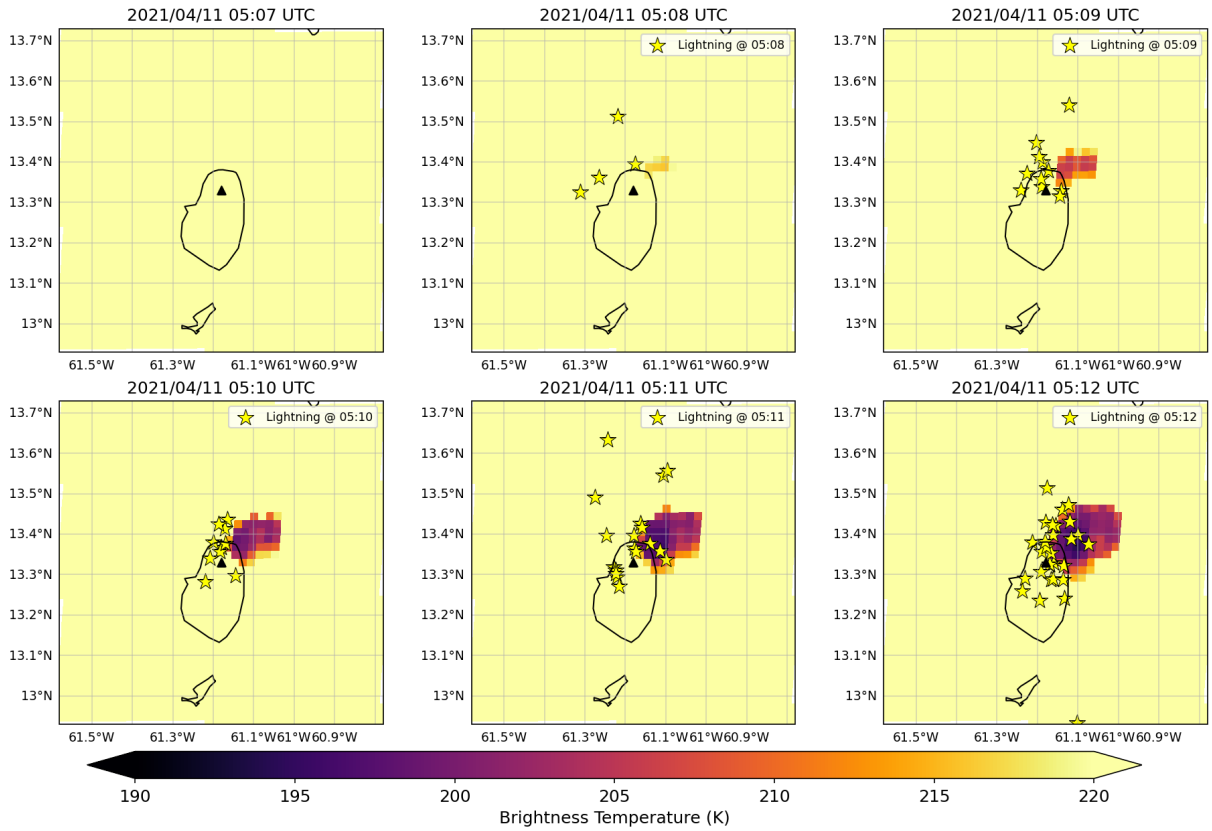

Figure 7: Lightning strikes (yellow stars) overlaid on GOES-16 ABI brightness temperature plume maps for Event 17 on 2021/04/11. Panels show frames $2-7$ (05:07-05:12 UTC) in 1-minute intervals with 43 lightning strikes around La Soufrière.

3.2 Classification and Mechanisms of Volcanic Lightning

Table 2 summarises the different known types of electrical activity associated with volcanic eruptions. These are typically categorised into vent discharges, near-vent lightning, and plume lightning, each characterised by distinct timescales, spatial extents, and onset conditions. Vent discharges occur within milliseconds of eruption onset and are confined to the vent region, often serving as early indicators of explosive activity [15]. Near-vent lightning follows shortly after and is linked to the sustained explosive phase, with discharges extending into the developing plume [15]. Plume lightning occurs several minutes after eruption onset and resembles thunderstorm lightning, with longer-duration flashes distributed throughout the stratified ash plume [15]. The rate and scale of electrical activity vary significantly between types, reflecting changes in eruption dynamics and particle interactions within the volcanic column. Unfortunately, WWLLN does not provide information on the type of lightning detected. This is because its sensors measure only the vertical component of the electric field from each lightning signal, and both cloud-to-ground and intra-cloud discharges appear very similar in this component [16]. As a result, the network cannot distinguish between the two. However, by comparing the timing

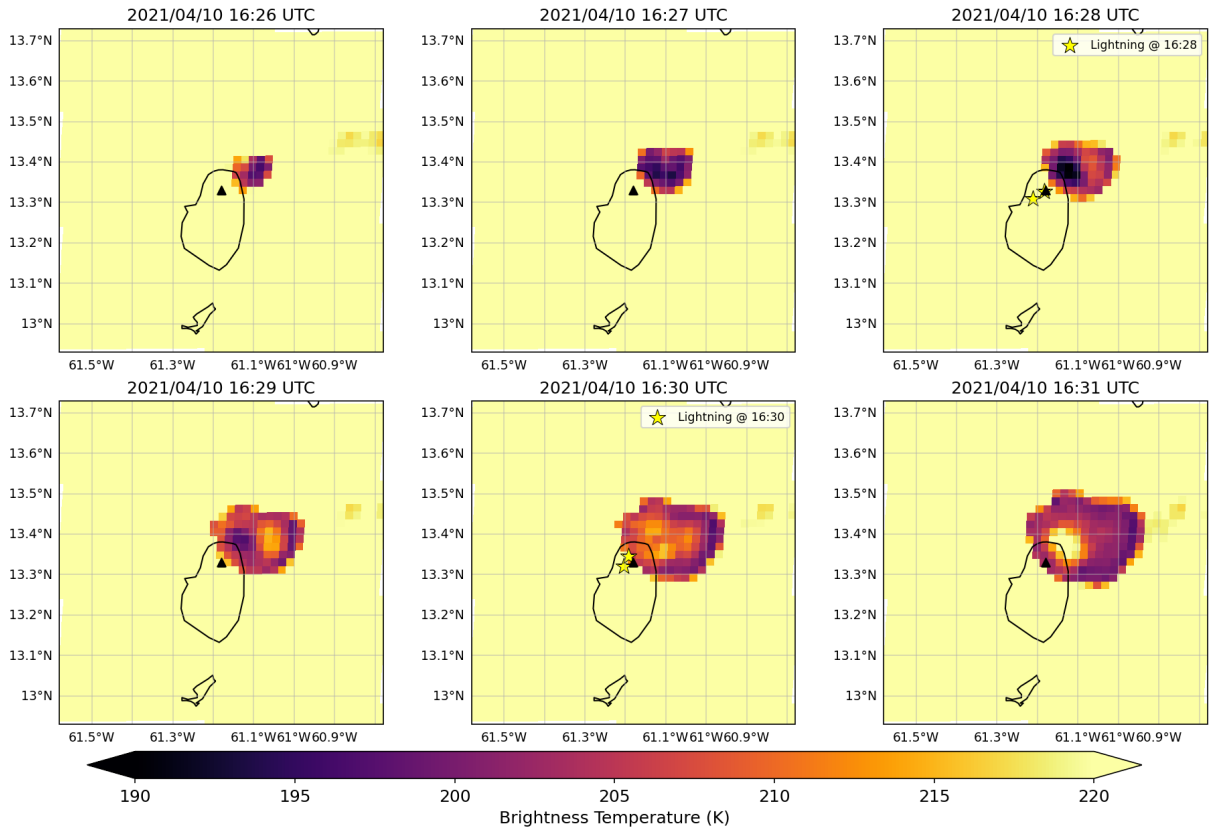

Figure 8: Lightning strikes (yellow stars) overlaid on GOES-16 ABI brightness temperature plume maps for Event 11 on 2021/04/10. Panels show frames $2-7$ (16:26-16:31 UTC) in 1-minute intervals around La Soufrière.

of strikes with the phase of the eruptive event, the strikes could be categorised.

The different types of volcanic lightning observed during eruptions are ultimately driven by the underlying charging mechanisms. These processes, and the spatial distribution of electrification within the volcanic plume, are summarised in Figure 9, which presents a schematic of proposed electrification mechanisms and the associated lightning types occurring in different plume regions. In the gas-thrust and near-vent regions, where ash generation and particle collisions are most intense, charging is dominated by processes such as fracto- and tribo-electrification. Higher in the plume, particularly in moist or water-rich eruptions, interactions between ash and hydrometeors and ice-related charging become more prominent. The figure also highlights how detection techniques vary with lightning type, and how each region contributes differently to monitoring applications such as ash detection and early warning systems.

To understand how and where these electrification mechanisms operate, it is first necessary to consider the physical processes involved in generating and transporting volcanic ash. Explosive volcanic eruptions fragment magma into tephra, transforming it from a mixture of crystals and

Table 2: Summary of the three types of lightning seen during volcanic eruptions [15].

Type	Duration	Scale	Onset & Conditions	Rate	Key Notes
Vent discharges	<1 ms	10-100 m	Within 1 s of eruption onset. Seen in eruptions with ash and gas only.	1–10 per ms	Radio frequency power similar to thunderstorm leader steps; indicator of active eruption; rate of discharges and tephra discharge rate link unverified.
Near-vent lightning	up to 30 ms	a few km	1–2 min after onset; detected whilst explosive phase is active; low-rate of discharge during weak ash output.	Occasional, accompanies vent discharges	Channels originate at vent and extend into plume
Plume lightning	10 ms - 1 s	sub-km to >20 km	Several minutes after onset, once plume is established.	Larger but less frequent as plume matures and becomes more stable and stratified.	Behaves like thunderstorm lightning with largest flashes occurring farthest from vent.

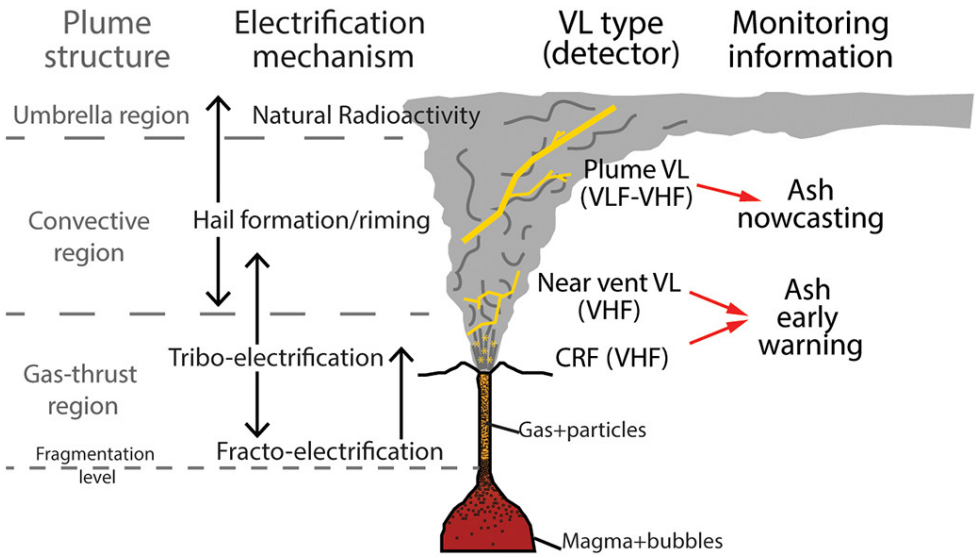

Figure 9: Schematic of proposed volcanic plume electrification mechanisms and the corresponding types of volcanic lightning (VL) observed in each region of the plume, along with the most suitable detection techniques. Fracto-electrification and tribo-electrification dominate near the gas-thrust region, producing continuous radio frequency (CRF) signals and near-vent lightning (VHF), while lightning in the upper convective and umbrella regions is associated with processes such as hail formation, riming, and natural radioactivity, producing plume lightning (VLF–VHF). [17]

gas bubbles suspended in a silicate melt into a turbulent suspension of ash and gas in the eruption column [17]. In this environment, ash particles, particularly those smaller than 2 mm, act as the primary charge carriers, with mechanisms including fracto-electrification, tribo-electrification, hydrometeor interactions, and natural radioactivity all contributing to plume charging [17]. These processes not only drive lightning generation but also influence ash behaviour: charged particles can clump together or settle more rapidly (aggregation and sedimentation) [18] [17], while particles retaining charge for longer may remain suspended, potentially influencing climate and the global electrical circuit [17].

Each charging mechanism has distinct physical origins. Fracto-electrification arises when materials fracture, generating charge through effects such as piezoelectricity and ion release, whereas tribo-electrification results from collisions between particles and depends on factors such as size, surface characteristics, and material heterogeneity. This often produces size-dependent bipolar charging, with smaller particles tending to acquire negative charge and larger ones positive charge [17]. Water plays a crucial role in plumes with high moisture content: ash–hydrometeor interactions can mimic thunderstorm charging processes, and volcanic ash can act as ice nuclei at high altitudes, further enhancing electrification through ice–ash interactions [19] [20] [21].

3.3 Investigating Atmospheric Profiles

It was initially hypothesised that atmospheric conditions during Event 17 may have played a role in enhancing the lightning activity observed, potentially by influencing the charging mechanisms involved. To investigate this, ECMWF reanalysis data was obtained for the region and vertical profiles of temperature, pressure, and water vapour were generated to assess whether there were significant differences in atmospheric conditions during the various events. Particular attention was given to water vapour content, as an increase in atmospheric moisture could contribute to enhanced electrification processes, thereby resulting in a higher frequency of lightning strikes.
Figure 10 presents the daily mean vertical temperature and pressure profiles for 10 April (top) and 11 April (bottom). The solid red trace denotes the ensemble-mean daily temperature (K) with the semitransparent band representing the variability of one standard deviation, while the blue trace indicates the pressure (hPa). The dashed red line marks the mean tropopause altitude (17.4 ± 0.4 km on 10 May versus 16.6 ± 0.3 km on 11 May) and the dotted cyan line the mean freezing-layer altitude (4.81 ± 0.04 km versus 4.96 ± 0.05 km). The close correspondence of both mean profiles and their respective standard deviation bands, differing only by a few tenths of a km, demonstrates that the thermal structure and dynamic layering of the upper troposphere and lower stratosphere remained essentially unchanged between these two consecutive days. The majority of variability on the 10th compared to the 11th occurred in the upper stratospheric levels, which should not affect any meteorological phenomena. Event 17 occurs on the morning of 11 May, and an hourly analysis of the vertical temperature and pressure profiles throughout that day (see the appendix) also shows negligible atmospheric variability.

Figure 11 compares the daily mean vertical water vapour profiles for 10 April (left) and 11 April (right). In both panels, the solid black line shows the ensemble-mean H_2O mixing ratio (ppmv) and the gray envelope its variability $\pm 1\sigma$. Near the surface, both days show very high moisture concentrations (≈ 25000 ppmv) that decrease sharply through the boundary layer ($1 - 3$ km), followed by a more gradual decline between 3-8 km where the variability peaks. Above ≈ 8 km, water vapour falls below 1000 ppmv and the profile becomes tightly constrained. The overall shape, magnitude and variability of the H_2O distributions are essentially indistinguishable between the two days, indicating a highly stable moisture structure in the upper troposphere. Note that this represents a large-scale view of the atmosphere and may not accurately capture local conditions. In this context, local weather data would provide more useful information (see Section 4).

3.4 Plausible reasons

With atmospheric interference ruled out, the observations suggest that a fundamental change occurred at the source. This is supported by the presence of a large shockwave associated with Event 17, as shown in Figure 12, which shows the shockwave progressing in four frames. The

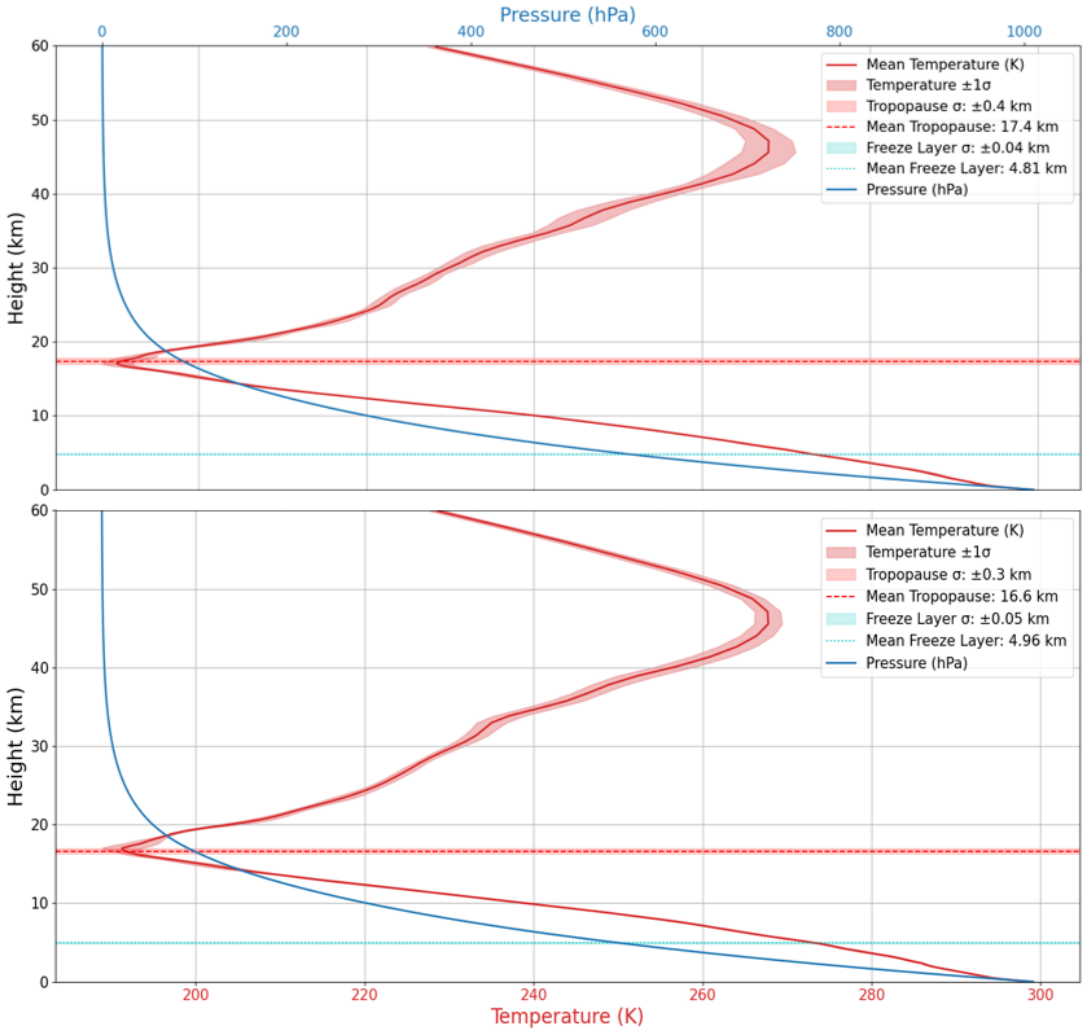

Figure 10: Daily mean vertical profiles of temperature and pressure for 10 April (top) and 11 April (bottom). The solid red line shows the ensemble-mean temperature (K) with shaded $\pm 1\ \sigma$ variability, and the solid blue line shows the pressure (hPa). The dashed red and dotted cyan horizontal lines indicate the mean tropopause and mean freezing-layer altitudes, respectively, with their own $\pm 1\ \sigma$ bands. The near-overlap of all curves and bands on both days highlights minimal day to day variability in the upper-tropospheric thermal structure and layer positions.

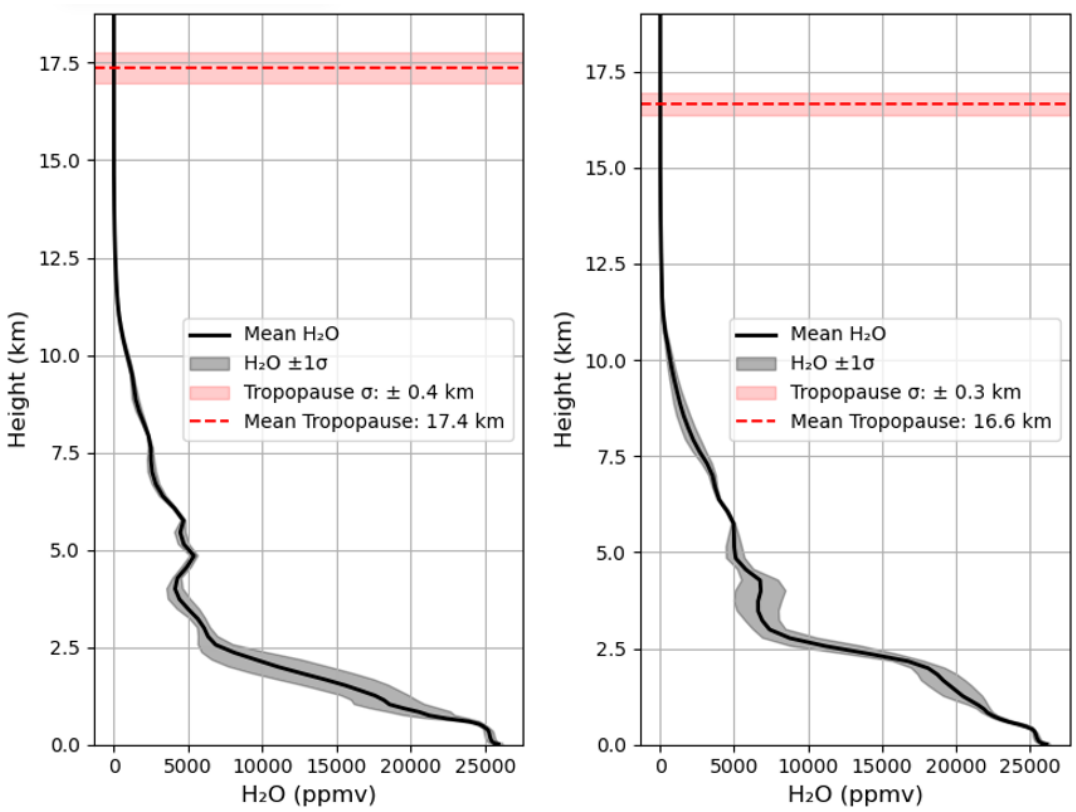

Figure 11: Daily mean vertical water-vapour profiles for 10 April (left) and 11 April (right), with the solid curve showing mean H_2O mixing ratio, grey shading indicating $\pm 1\sigma$ variability, and the dashed line marking the tropopause. The near-identical shapes and spreads between panels highlight minimal day to day changes in moisture structure.

figure was created by comparing two consecutive brightness temperatures and choosing a highly contrasting scale. The shockwave was reported to have cut power across the island, indicating the considerable intensity of the event [22]. Notably, Event 17 occurred nearly 41 hours after the initial explosion, during a period when the magma supply rate was already in decline [23]. Although the precise cause of this change remains unknown, it may provide a potential link between certain volcanic processes and the observed enhancement of plume electrification.

Van Eaton et al. [24] investigated the lightning activity during the 2015 eruption of Calbuco in Chile, noting that of the two eruptive phases identified, the second produced approximately ten times more lightning strokes than the first [24]. Observations showed that the volcanic cloud in the second phase expanded more rapidly, indicating an eruption rate approximately 50% greater than in the first phase, and that the umbrella cloud ceased its upwind expansion despite the eruption continuing and no significant changes in the background wind field [24]. The halt in upwind spreading, followed by cloud recession, implied a reduced mass flux feeding the umbrella. Coinciding with this change, the number of proximal lightning strokes increased sharply. While

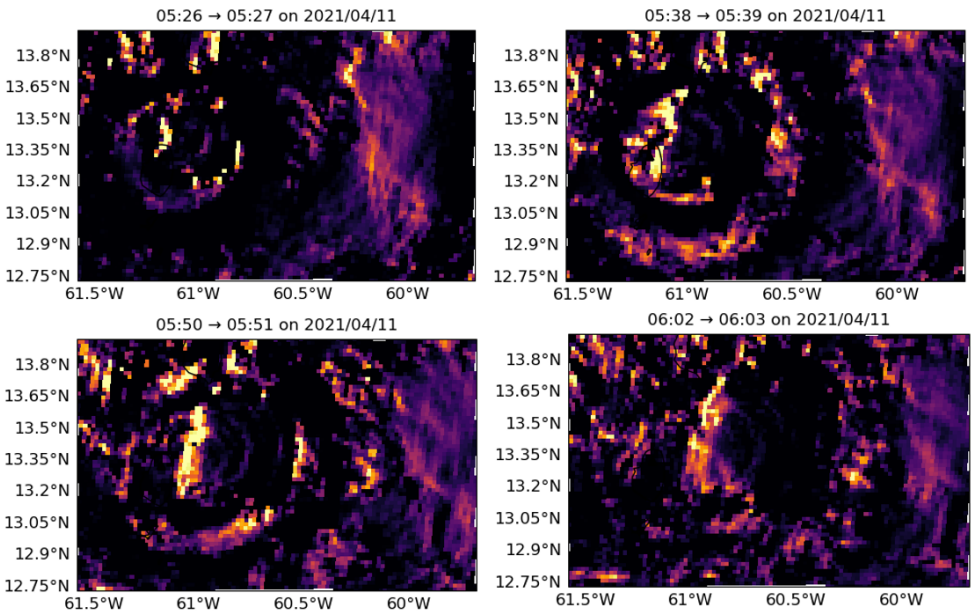

Figure 12: Frames showing a shockwave progressing through the region associated with Event 17.

higher lightning rates have been associated with expanding cloud size [25] [26], the abrupt rise in proximal strikes suggested an impulsive change at the source [24]. Van Eaton et al. hypothesised that this lightning was triggered by pyroclastic density currents (PDCs) [24].

PDCs are hot, ground-hugging flows of ash and debris that can travel at speeds of hundreds of metres per second, reaching many tens to hundreds of kilometres from the source [27]. Van Eaton et al. suggested that low-level ash clouds near the PDCs could introduce a new atmospheric charge layer capable of triggering cloud-to-ground lightning [24]. PDCs also occurred during the eruption of La Soufrière and so could be a mechanism for generating the lightning observed in Event 17. Partially carbonised trees washed up at Chateaubelair at midday on 11 April provided evidence that pyroclastic density currents had taken place earlier that day or on the evening of 10 April, with additional PDC activity occurring on 11 April [22]. The timings of these PDCs were difficult to determine and were estimated by analysing a figure from Cole et al. The closest timings obtained to Event 17, which began at 05:05 UTC, were 03:27, 05:59, and 08:53 UTC [22]. These estimates are approximate because they were derived from a figure rather than from a table. Nevertheless, none of these timings are closely aligned with the start time of Event 17. Therefore, it cannot be conclusively stated that PDCs were the sole cause of the intense electrical activity observed during Event 17.

Another possible explanation is that Event 17 was unusually intense, as indicated by the prominent shockwave. Such an event could have caused rapid ash fragmentation, enhancing both fracto- and tribo-electrification processes. In a study of the Sakurajima volcano in Japan,

Cimarelli et al. [17] found that the number of lightning discharges was proportional to the pressure measured by infrasound stations, demonstrating a positive correlation between electrical activity and explosion intensity [17]. If pressure readings had been available for the different events at La Soufrière, this relationship could have been tested directly - a topic for future work. Nonetheless, the observed shockwave suggests that the explosion was highly energetic and would likely have produced a higher pressure reading than the other events.

3.5 Height estimates

The initial objective of this project was to use volcanic lightning as a proxy to estimate plume heights in all eruptive events. Due to insufficient lightning strikes for most events, this approach was only applied to Event 17. A parallax adjustment was applied to the lightning strike locations to account for the satellite viewing geometry and the assumed plume height. Without this correction, the lightning strikes would not align spatially with the volcanic cloud, as the apparent cloud position in the satellite imagery is displaced by the viewing geometry. Without this adjustment, the strikes and plume would appear in different spatial planes. Several strikes were observed in apparent isolation from the plume, but close to the volcano (e.g. Figure 7) , suggesting that their recorded positions were the result of parallax displacement. To constrain the heights of the plumes, the strike positions were iteratively adjusted for column heights between 5 km and 25 km, and the number of strikes located inside versus outside the plume were recorded for each height. This process was performed at one-minute intervals for Event 17 to examine temporal changes in plume height. Figure 13 presents the strike frequency as a function of parallax-corrected height for six individual minutes during Event 17. At 05:12 UTC, the distribution suggests a plume height between 13–18 km, with a secondary maximum near 23 km. At 05:13 UTC, the range of possible heights broadens to 13–19 km, again with a peak near 22 km. During 05:14-05:15 UTC, maximum strike counts (approximately 20) correspond to heights between 19 and 21 km, with some association with the range of 16 to 21 km. By 05:16–05:17 UTC, the estimated range expands, indicating potential plume heights between 13 and 25 km. These results demonstrate both temporal variability and inherent uncertainty in height estimation using parallax adjustment on lightning strikes. This method could be further explored in the future.

4 Discussion

Overall, the analysis of volcanic lightning during this eruption was constrained by both the incompleteness of the datasets and the limited availability of data. In the case of WWLLN, only approximately 15–30% of strokes detected by a single sensor are recorded by at least five sensors, which is a requirement for accurate geolocation [6]. These detections predominantly correspond to higher peak-current strokes. Recent studies estimate the global detection efficiency for strokes of approximately 30 kA to be around 30% [6]. While WWLLN is capable of detecting both

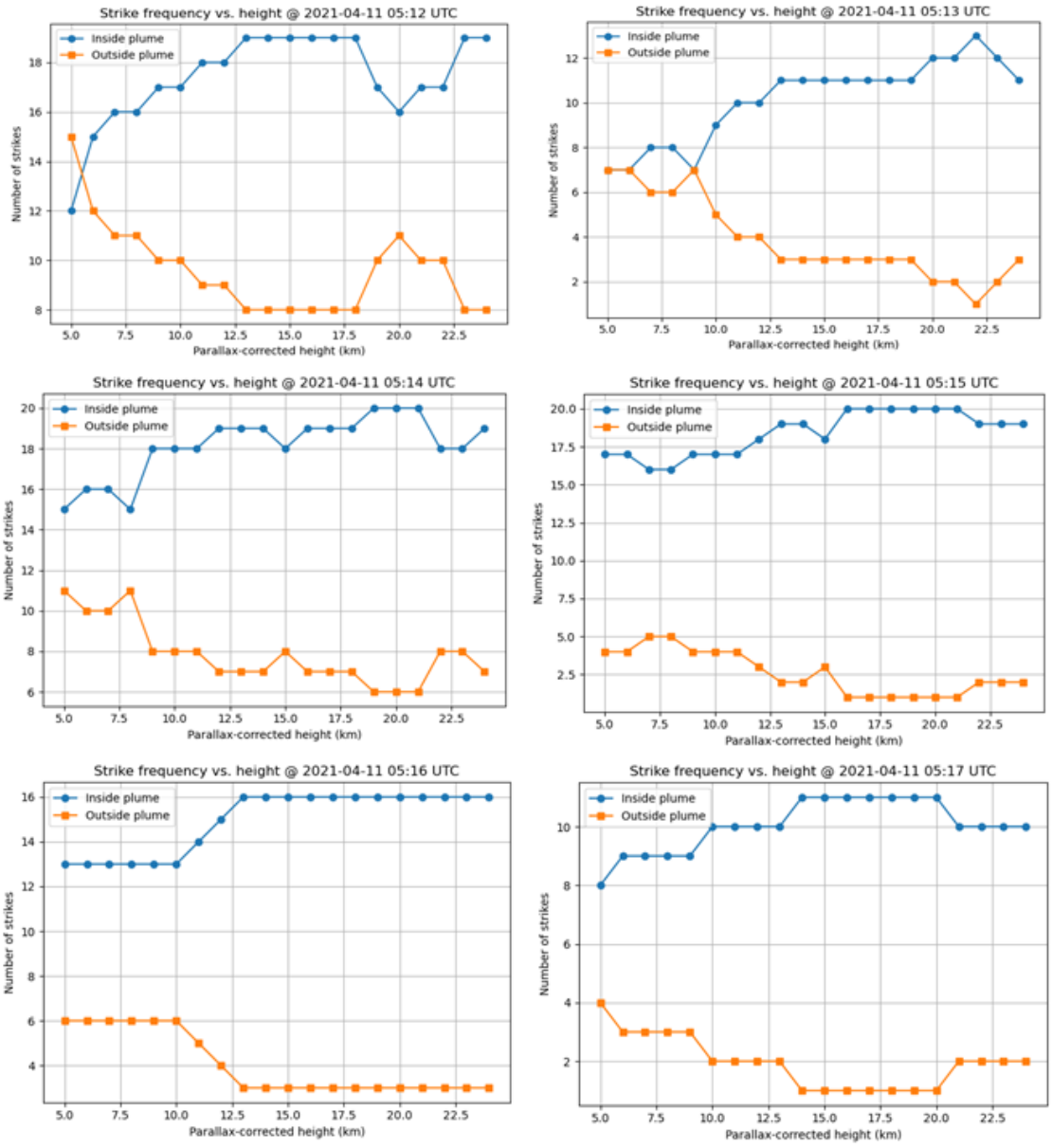

Figure 13: A plot of strike frequency versus parallax-corrected height for six consecutive times during Event 17. The plot shows the number of strikes within the plume at each time, as well as the number of strikes occurring outside the plume.

cloud-to-ground and intra-cloud lightning, the lower peak currents characteristic of intra-cloud discharges mean that the network is inherently more sensitive to cloud-to-ground events [8]. Consequently, it is plausible that a proportion of lightning activity during the eruptions was not detected. Furthermore, WWLLN does not distinguish between lightning types in its data products; however, given its detection bias, it is reasonable to assume that the majority of detected strokes were cloud-to-ground. The deployment of a Lightning Mapping Array (LMA) would have provided benefits in this context, offering high-resolution three-dimensional lightning channel mapping with meter-scale spatial accuracy and microsecond temporal resolution, allowing a more detailed characterisation of lightning structure and electrification processes [28]. Its capability to reconstruct the three-dimensional structure of lightning strokes would significantly enhance plume height analysis.

The study of volcanic lightning in this eruption has provided valuable insights into plume dynamics and electrification processes. The availability of lightning strike data in the vicinity of an eruption provides an additional indicator that volcanic activity has occurred, which is particularly beneficial in remote or inaccessible regions. The occurrence of volcanic lightning also strongly suggests the formation of an ash-bearing plume. If the onset of an eruption is defined by the start of seismic activity, volcanic lightning typically follows shortly after, provided the eruption has an ash bearing volcanic plume, as shown in Table 3. Although the time differences between the seismic and lightning onsets vary considerably, they are generally close enough to be operationally useful. When the eruption onset is instead defined by the first visual detection of an ash plume, this time discrepancy can be reduced to only a few minutes.

Lastly, access to local weather data for the region would have been advantageous, as large-scale atmospheric analyses may not properly capture localised conditions. Such data could help determine whether a small-scale thunderstorm was present or provide evidence relevant to the increase in pressure leading to an increase in lightning strikes hypothesis. The nearest free to use available dataset consisted of atmospheric soundings from Grantley Adams International Airport in Barbados, provided by the University of Wyoming [29]. These soundings indicated no unusual atmospheric features; however, the site's distance from Saint Vincent limits the applicability of these observations.

5 Conclusions

The analysis highlights the value of volcanic lightning as a complementary tool for monitoring explosive eruptions, particularly when integrated with high-resolution satellite observations. Despite WWLLN's limitations in detection efficiency and stroke classification, the timing and distribution of lightning relative to plume development provided useful insights into eruption onset and intensity. Event 17 stood out for its exceptionally high lightning activity, which could not be explained by meteorological factors and was more likely associated with changes in erup-

Table 3: Seismic and lightning start times per event, and their difference (Δt = lightning start − seismic start).

Event	**Day**	**Seismic start (HH:MM)**	**Lightning start (HH:MM)**	Δt **(min)**
6	10	09:35	09:56	21.0
7		10:47	10:59	12.0
8		12:02	12:20	18.0
9		12:54	13:15	21.0
10		14:27	14:44	17.0
11		16:20	16:28	8.0
12		18:50	18:51	1.0
13		21:20	21:34	14.0
14		23:02	23:11	9.0
15	11	00:51	01:07	16.0
16		02:44	02:54	10.0
17		04:59	05:08	9.0
18		07:55	08:23	28.0
19		10:36	11:13	37.0
20		13:24	14:07	43.0
21		18:20	18:13	-7.0
22		20:22	20:18	-4.0
23	12		01:19	
24		00:39	01:19	40.0
25		07:59	08:18	19.0
26				
27		20:53		
28	13	10:23	10:37	14.0
29	14		00:53	
30		02:27	02:53	26.0
31		15:31	16:08	37.0
32	15			
33	16	10:16		

tive dynamics, including a strong shockwave and rapid ash fragmentation. Parallax-corrected lightning positions suggested plume heights of 13–25 km during this event, demonstrating both the feasibility and uncertainty of deriving plume geometry from lightning data. The study also emphasises the advantages of more advanced systems, such as Lightning Mapping Arrays, which offer three-dimensional lightning channel mapping and higher detection efficiency. Ultimately, volcanic lightning observations, when combined with other geophysical datasets, can improve real-time eruption detection, contribute to hazard assessment, and enhance our understanding of plume electrification processes in both volcanic and meteorological contexts.

6 Acknowledgements

Lightning data for the eruption is found freely on the WWLLN website at `https://wwlln.net/USGS/Global/`. Seismic start times were taken from Sparks et al. [23], specifically Table 1, who declared that the datasets generated and analysed are available from the Seismic Research Centre at the University of the West Indies. A big thanks to Isabelle A. Taylor, who provided numerous codes and pre-processed data, including GOES-16 satellite data available through NOAA's Big Data Program (`https://www.noaa.gov/informationtechnology/open-data-dissemination`; NOAA, 2022), and meteorological data available from ECMWF. A further big thanks to Don Grainger and the rest of EODG, including the summer students who all pitched in ideas and suggestions.

References

[1] Global Volcanism Program, "Report on La Soufrière (Saint Vincent) (West Indies)." `https://volcano.si.edu/volcano.cfm?vn=360150`, 2021. Accessed: 2025-07-29.

[2] E. P. Joseph, M. Camejo-Harry, T. Christopher, R. E. A. Robertson, T. Syers, J. L. Latchman, S. Elstow, and S. C. Loughlin, "Responding to eruptive transitions during the 2020–2021 eruption of la soufrière volcano, st. vincent," *Nature Communications*, vol. 13, no. 1, p. 4129, 2022.

[3] I. A. Taylor, R. G. Grainger, A. T. Prata, S. R. Proud, T. A. Mather, and D. M. Pyle, "A satellite chronology of plumes from the april 2021 eruption of la soufrière, st vincent," *Atmospheric Chemistry and Physics*, vol. 23, no. 24, pp. 15209–15234, 2023.

[4] J. R. Dwyer and M. A. Uman, "The physics of lightning," *Physics Reports*, vol. 534, no. 4, pp. 147–241, 2014.

[5] EEEGUIDE, "Lightning." `https://www.eeeguide.com/lightning/`. Accessed: 18-Aug-2025.

[6] World Wide Lightning Location Network, "How it works." `https://wwlln.net/`, 2025. Accessed: 2025-07-25.

[7] Radartutorial, "Multilateration." https://www.radartutorial.eu/02.basics/rp52.en.html. Accessed: 18-Aug-2025.

[8] J. Rodger, C. and et al., "Location accuracy of VLF World-Wide Lightning Location Network," technical report, University of Washington, 2005.

[9] World Wide Lightning Location Network, "Ash Cloud Monitor (ACM)." https://wwlln.net/volcanoMonitor.html, 2025. Accessed: 2025-07-25.

[10] World Wide Lightning Location Network, "Global Volcanic Lightning Monitor." https://wwlln.net/USGS/Active/, 2025. Accessed: 2025-07-25.

[11] NASA Earthdata, "Abi – advanced baseline imager." https://www.earthdata.nasa.gov/data/instruments/abi, 2025. Accessed: 1-Aug-2025.

[12] M. J. Pavolonis, J. M. Sieglaff, and J. L. Cintineo, "Chapter 10 - remote sensing of volcanic ash with the goes-r series," in *The GOES-R Series* (S. J. Goodman, T. J. Schmit, J. Daniels, and R. J. Redmon, eds.), pp. 103–124, Elsevier, 2020.

[13] T. Schmit, J. Gurka, W. Menzel, and M. Gunshor, "Introducing the next generation geostationary imager - goes-r's advanced baseline imager (abi)," *Conference on Satellite Meteorology and Oceanography*, 01 2004.

[14] NOAA/NASA GOES-R Series, "Advanced baseline imager (abi) scan & imaging modes." https://www.goes-r.gov/spacesegment/abi.html, 2025. Accessed: 1-Aug-2025.

[15] S. R. McNutt and R. J. Thomas, "Chapter 62 - volcanic lightning," in *The Encyclopedia of Volcanoes (Second Edition)* (H. Sigurdsson, ed.), pp. 1059–1067, Amsterdam: Academic Press, second edition ed., 2015.

[16] E. A. Navarro, J. A. Portí, A. Salinas, S. Toledo-Redondo, J. Segura-García, A. Castilla, V. Montagud-Camps, and I. Albert, "The world wide lightning location network (wwlln) over spain," *Natural Hazards and Earth System Sciences*, vol. 24, no. 11, pp. 3925–3943, 2024.

[17] C. Cimarelli and K. Genareau, "A review of volcanic electrification of the atmosphere and volcanic lightning," *Journal of Volcanology and Geothermal Research*, vol. 422, p. 107449, 2022.

[18] J. Taddeucci, P. Scarlato, C. Montanaro, C. Cimarelli, E. Del Bello, C. Freda, D. Andronico, M. Gudmundsson, and D. Dingwell, "Aggregation-dominated ash settling from the eyjafjallajökull volcanic cloud illuminated by field and laboratory high-speed imaging," *Geology*, vol. 39, pp. 891–894, 09 2011.

[19] C. Textor, H.-F. Graf, M. Herzog, and J. M. Oberhuber, "Injection of gases into the stratosphere by explosive volcanic eruptions," *Journal of Geophysical Research*, vol. 108, no. D19, 2003. Art. no. D19.

[20] A. J. Durant, R. A. Shaw, W. I. Rose, Y. Mi, and G. G. J. Ernst, "Ice nucleation and overseeding of ice in volcanic clouds," *Journal of Geophysical Research*, vol. 113, no. D9, 2008.

[21] K. Genareau, S. Cloer, K. Primm, M. Tolbert, and T. Woods, "Compositional and mineralogical effects on ice nucleation activity of volcanic ash," *Atmosphere*, vol. 9, no. 7, p. 238, 2018.

[22] P. D. Cole, J. Barclay, R. E. A. Robertson, S. Mitchell, B. V. Davies, R. Constantinescu, R. S. J. Sparks, W. Aspinall, and A. Stinton, "Explosive sequence of la soufrière, st vincent, april 2021: insights into drivers and consequences via eruptive products," *Geological Society, London, Special Publications*, vol. 539, no. 1, pp. 81–106, 2024.

[23] S. R. J. Sparks, W. P. Aspinall, J. Barclay, I. A. Renfrew, R. Contreras-Arratia, and R. Stewart, "Analysis of magma flux and eruption intensity during the 2021 explosive activity at la soufrière, st vincent, west indies," *Geological Society, London, Special Publications*, vol. 539, no. 1, pp. 63–79, 2024.

[24] A. R. Van Eaton, A. Amigo, D. Bertin, L. G. Mastin, R. E. Giacosa, J. González, O. Valderrama, K. Fontijn, and S. A. Behnke, "Volcanic lightning and plume behavior reveal evolving hazards during the april 2015 eruption of calbuco volcano, chile," *Geophysical Research Letters*, vol. 43, no. 7, pp. 3563–3571, 2016.

[25] E. R. Williams, "Large-scale charge separation in thunderclouds," *Journal of Geophysical Research: Atmospheres*, vol. 90, no. D4, pp. 6013–6025, 1985.

[26] S. A. Behnke and E. C. Bruning, "Changes to the turbulent kinematics of a volcanic plume inferred from lightning data," *Geophysical Research Letters*, vol. 42, no. 10, pp. 4232–4239, 2015.

[27] British Geological Survey, "Understanding the dynamics of pyroclastic density currents." `https://www.bgs.ac.uk/geology-projects/volcanoes/pyroclastic-density-currents/`, 2025. Accessed: 15-Aug-2025.

[28] "Lightning mapping array (lma)." `https://www.earthdata.nasa.gov/data/instruments/lma`, 2025. Accessed: 2025-08-15.

[29] "Atmospheric soundings – wyoming weather web: Legacy interface." `https://www.weather.uwyo.edu/upperair/sounding_legacy.html`, 2025. Accessed: 2025-08-15.